Bio-oil as a source of renewable chemicals: the chemistry of pyrolytic lignin

Wenes Ramos Silva[1] · Tarcisio Martins Santos[1] · Jhonattas Carvalho Carregosa[1] · Caroline Carriel Schmitt[2] · Klaus Raffelt[2] · Nicolaus Dahmen[2] · Alberto Wisniewski Jr[1]

Abstract

Pyrolytic lignin from beech wood bio-oil was fractionated into low molecular mass (LMM) and high molecular mass (HMM). A comprehensive characterization by FTIR, GPC, TG, GC/MS, and multidimensional NMR spectroscopy was employed to analyze the individual fractions. Additionally, advanced characterization was carried out using ultra-high-resolution mass spectrometry (UHRMS). The data reveal that the LMM fraction has a higher prevalence of phenolic monomers due to homolytic cleavage of the RC−OAr linkage in aryl−O−alkyl ether bonds corroborating with GC/MS results. On the other hand, the HMM fraction shows a higher degree of polymerization and a wider molecular mass distribution, predominantly comprising carbohydrate derivatives by GC/MS. UHRMS data proved to be valuable in characterizing the monomers and oligomers present in each fraction, offering insights for future applications and the development of value-added products. Overall, this work significantly advances the current knowledge of pyrolytic lignin structures, opening opportunities for innovative technological bioproducts.

Keywords Biochemicals · Phenolic compounds · Bio-oilomics · Biopolymers · Biomass · Lignocellulosic

1 Introduction

Concerns related to the depletion of petroleum reserves and our society's increasing dependence on energy and industrial chemical inputs have driven researchers to develop alternative technologies aimed at converting renewable resources into more sustainable energy and industrial application products [1]. Among the variety of technologies under development nowadays, the conversion of lignocellulosic biomass through fast pyrolysis process is considered one of the most promising possibilities for the reduction of fossil carbon consumption [2]. Lignocellulosic biomass is the most abundant, sustainable, and inexpensive carbon source that can be used to produce renewable-based fuels and chemicals. It is formed through the photosynthesis reactions that produce

✉ Alberto Wisniewski Jr
albertowj@academico.ufs.br

1 Petroleum and Energy from Biomass research group (PEB), Federal University of Sergipe (UFS), Av. Marcelo Déda Chagas sn. 49107 230, São Cristóvão, SE, Brazil

2 Institute of Catalysis Research and Technology, Karlsruhe Institute of Technology, 76344 Karlsruhe, Germany

plant fibers, consisting of macromolecular substances that are held together by a polysaccharide matrix called holocellulose, composed of cellulose and hemicellulose, and a recalcitrant polymeric layer known as lignin [3–5].

During fast pyrolysis, the building blocks of biomass are decomposed, resulting in a viscous, highly oxygenated brown liquid denominated bio-oil [6]. Because of the poor thermal stability of the holocellulose matrix, it decomposes between 215 and 400 °C producing a wide range of compounds such as carbohydrate derivatives (pentoses, hexoses, furans, and levoglucosan), sugar oligomers, and short-chain compounds belonging to the classes of carboxylic acids, alcohols, aldehydes, and ketones. Lignin, a macromolecule responsible for mechanical strength of the plants (composed of three main aromatic monomers building blocks: guaiacyl (G), syringyl (S), and p-hydroxyphenyl (H)) is decomposed in the range of 160 to 900 °C producing low and high molecular mass phenolic compounds [2, 7]. Due to α- and β-ether bonds of lignin, which will cleave spontaneously at high temperatures (especially above 300 °C), depolymerization of lignin occurs during pyrolysis process. However, due to the short residence time of the biomass in the fast pyrolysis reactor, up to 5 s, the lignin polymer matrix is only partially

decomposed [8]. Furthermore, repolymerization reactions occur rapidly via a quinone methide intermediate formed from a conjugated C=C structure of the product, yielding higher molecular mass products, which eventually results in the formation of solid residues [9]. In this way, approximately 30% of the fast pyrolysis bio-oil composition is what is called "pyrolytic lignin," fragments of different molecular mass obtained due to the partial fragmentation of lignin. The presence of pyrolytic lignin is associated with bio-oil instability, leading to increased viscosity and posing challenges for its further processing and upgrading [10, 11].

Another challenge faced by the presence of pyrolytic lignin in the bio-oil is the current technology for fractionating bio-oil. Among the fractionation forms, the distillation of bio-oil has the restraint caused by the polymerization of bio-oil [1]. Despite its disadvantage in bio-oil, pyrolytic lignin presents itself as an intriguing feedstock, particularly when targeting aromatic building blocks. This is due to its substantial carbon content and inherent aromatic structures, which render it a renewable resource with significant potential for producing high-value chemicals [1]. Therefore, the separation of pyrolytic lignin from bio-oil can be a viable alternative to overcome the aforementioned challenges. To recover pyrolytic lignin from bio-oil, water can be employed as an extraction medium, since its chemical structure makes it insoluble in water [12]. In addition, different organic solvents can be used to carry out subsequent fractionation of the pyrolytic lignin [13] which allows a more detailed characterization of this type of sample, offering a viable alternative approach for the use of this fraction of bio-oil in obtaining innovative technological bio-products. The exploration and utilization of alternative renewable raw materials as monomer sources for the chemical industry is a step towards sustainable development. The isolation of pyrolytic lignin presents an opportunity to increase the recovery of phenolic monomers, which can be used to produce other high-value compounds, thereby enhancing economic returns. Phenolic derivatives have industrial applications in pharmaceutical, cosmetic, textile, packaging, and food areas [14], as well as in the production of phenolic resins, which are employed in various industries [15]. Overall, the isolation and utilization of pyrolytic lignin represent a promising strategy to maximize the value of lignocellulosic biomass through the pyrolysis process. Environmental concerns and the need to reduce our dependency on petroleum-based chemicals create a new demand for bio-based chemicals [16].

The characterization of pyrolytic lignin plays a crucial role in predicting reaction mechanisms and proposing transformation pathways to maximize its conversion into value-added chemicals [17]. Various analytical techniques are commonly employed for lignin structure characterization, including elemental analysis, Fourier transform infrared spectroscopy (FTIR), gel permeation chromatography

(GPC), thermographic analysis (TG), online pyrolysis with gas chromatography/mass spectrometry (Py−GC/MS), and ^{1}H−^{13}C nuclear magnetic resonance (HSQC NMR) [18]. In addition to these techniques, the drive to enhance the characterization and comprehension of this intricate biopolymer has fostered the development of diverse analytical approaches, which center on high-resolution mass spectrometry and subsequent data analysis. Within this analytical technique, soft atmospheric ionization methods can be employed to ionize the compound while preserving the integrity of lignin oligomers, facilitating direct analysis without the need for complex sample preparation steps or prior chromatographic separation. This analysis provides valuable insights into trends, compound series, chemical classes, and analytical information pertaining to lignin substructures. Moreover, this approach obviates the necessity for lignin structure degradation, thereby enabling a more comprehensive understanding of this natural polymer [19].

This work focuses on the characterization of pyrolytic lignin isolated from the bio-oil obtained through fast pyrolysis of beech wood. The pyrolytic lignin was further fractionated into low molecular mass and high molecular mass fractions using dichloromethane (DCM). Given the complex nature of lignin, a range of analytical techniques was employed to gain insights into the structure of the samples. To comprehensively analyze the individual fractions, classical lignin characterization techniques such as Fourier transform infrared spectroscopy (FTIR), gel permeation chromatography (GPC), thermogravimetry (TG), gas chromatography/mass spectrometry (GC/MS), and multidimensional NMR spectroscopy were utilized. Additionally, advanced comprehensive characterization was performed using ultra-high-resolution mass spectrometry (UHRMS). The combined application of these characterization techniques enabled the extraction of valuable information regarding the structure of the pyrolytic lignin obtained. This thorough approach is expected to enhance the current understanding of the structures and composition of the pyrolytic lignin given support to the potential use of lignin in biorefineries platform [20].

2 Methodology

2.1 Isolation of low molecular mass (LMM) and high molecular mass (HMM) pyrolytic lignins

The beech wood bio-oil (BWBO), obtained by fast pyrolysis, was provided by BTG Biomass Technology Group BV, Netherlands. The BWBO exhibited spontaneous phase separation after storage (24 h at 80 °C), yielding an upper aqueous fraction and a lower organic fraction. The aqueous fraction accounted for 59 wt% of the total bio-oil, while the organic

fraction constituted 41 wt%. Both fractions presented a dark brown color. Notably, the organic fraction displayed significantly higher viscosity compared to the aqueous fraction. The pyrolytic lignin (PyL) extraction was conducted using the organic fraction of the BWBO, as the PyL is mainly concentrated in this fraction [21]. The fractionation of PyL for analytical proposal followed the previous literature based on the solubility of the structures by the molecular mass [22, 23].

Approximately 40 g of organic fraction was added dropwise to an ice-water mixture (130 g of ice and 270 g water) kept at 0.5–1 °C, under constant stirring (Ultra-Turrax T25, IKA, max. speed of 25,000 min^{-1}). The hydrophobic components, PyL, was then precipitated and vacuum filtrated (white stripe quantitative filter). The water insoluble fraction (PyL) was dried in a freezing drying (Alpha 2–4 LSC-plus, Martin Christ) at -87 °C and -0.035 mbar overnight. The solid fraction obtained was extracted with DCM in a proportion of 1:7 (in an ultrasound bath for 15 min, followed by vacuum filtration). The solid residue obtained is the PyL-DCM$_{Insol.}$ (HMM) and the soluble fraction (after solvent evaporation) is the PyLDCM$_{Sol.}$ (LMM). The content of extractives and solids were also determined as they usually are concentrated together with both LMM and HMM fractions. The extractives were determined by extraction with n-hexane, being the extractives the n-hexane soluble fraction while the solids were determined by the methanol insoluble fraction.

2.2 Characterization of low and high molecular mass pyrolytic lignin fractions

Both PyL fractions were analyzed in terms of elemental analysis, heating value, functional groups, molecular mass distribution, and thermal stability. Furthermore, for a more comprehensive characterization, the LMM and HMM samples were also characterized by gas chromatography/mass spectrometry (GC/MS), two-dimensional nuclear magnetic resonance spectroscopy (2D-NMR), and ultra-high resolution mass spectrometry (UHRMS). The procedures used in each analysis are detailed below.

2.2.1 Elemental analysis and high heating value (HHV)

The LMM and HMM fractions were analyzed following the same methodology. The carbon (C), nitrogen (N), and hydrogen (H) content of the samples was determined through elemental analysis, utilizing a LECO CHN628 elemental analyzer. The obtained results were processed using LECO CHN628 Software ver. 1.30 (St. Joseph, MI, USA). The instrument operated by employing helium (99.995%) and oxygen (99.99%) gases, with the furnace temperature set at 950 °C and the post-firing temperature at 850 °C. Additional

parameters were adjusted to enhance sensitivity. The equipment was calibrated with an EDTA standard (41.0% C, 5.5% H, and 9.5% N) using a mass range between 10 and 200 mg. The samples were analyzed using 50.0 mg on tin foil. The high heating value (HHV) was performed using a calorimeter IKA C5003 with a C551 cooling system.

2.2.2 Fourier transform infrared spectroscopy-attenuated total reflectance analysis (FTIR-ATR)

To obtain information about the functional groups present in the low LMM and HMM high molecular mass pyrolytic lignin fractions, the samples were also analyzed using a Bruker FTIR-ATR spectrometer (Alpha) using a diamond single reflection attenuated total reflectance (ATR). These measurements were carried out at the Instituto Superior de Agronomia (ISA), University of Lisbon. The spectra were measured in the wavenumbers from 4000 to 400 cm^{-1}.

2.2.3 Distribution of molecular mass by gel permeation chromatography (GPC)

An estimation of the distribution of the molecular mass was obtained by GCP measurements. Approximately 10 mg of both samples was diluted in 10 mL of Tetrahydrofuran (THF) and filtrated using a 0.2-µm PTFE filter. The samples were then injected (temperature: 37 °C; flow rate: 1 mL min^{-1}) to the equipment (Merck Hitachi, L-6200 Intelligent pump) with a Refractive Index Detector (Merck, LaChrom L-7490). The device was composed of two columns (length: 300 mm; inner diameter: 8 mm) packed with PSS SDV-gel, with different pore sizes (1000 Å and 100Å) and 5 µm of particle size. Before the measurements, the equipment was calibrated using polystyrene standards diluted in THF, using toluene as internal standard.

2.2.4 Thermogravimetric analysis (TG)

The evaluation of the thermal stability of PyL samples (LMM and HMM) was measured by thermogravimetric analysis using a TGA-50 thermogravimetric analyzer (Shimadzu, TA, America) under an atmosphere of N$_2$ with a flow rate of 50 mL min^{-1}. For this purpose, approximately 6 mg of sample were placed in a platinum crucible and heated from an initial temperature of 30 °C up to 1,000 °C under the heating rate of 10 °C min^{-1}, had its mass loss analyzed.

2.2.5 Characterization of volatile components present in PyL fractions and analysis of HMM fragments by GC/MS

Stock solutions of LMM and HMM (5 mg mL^{-1}) were produced by diluting the samples in previously distilled THF.

Aliquots of 80 µL of the stock solutions were further derivatized by adding 20 µL of N,O-bis(trimethylsilyl)trifluoroacetamide (BSTFA). The mixture was homogenized using a vortex and allowed to stand at 65 °C for 45 min, after which it was sent for analysis by gas chromatography/mass spectrometry (GC/MS).

Assuming that the HMM pyrolytic lignin fraction is mostly composed of nonvolatilizable oligomeric compounds, the HMM sample was subjected to a thermal cracking process aiming at a better understanding of the building units that compose the oligomeric structures present in the matrix in question. For this purpose, 100 mg of HMM was pyrolyzed using a microscale reactor operating at a temperature of 500 °C, following the methodology described in the work of Santos et al. [24]. The liquid product, herein referred to as PyHMM, was collected by elution from the reactor tube with THF and collected in a 5-mL volumetric flask. Subsequently, the concentration of the Py-HMM solution in THF was adjusted to obtain a final concentration of 5 mg mL^{-1}, which was subjected to the same derivatization process described above and subsequently analyzed by GC/MS.

Analysis of the PyL fractions and Py-HMM was performed using a Thermo Fisher Scientific TRACE 1310/TSQ 9000 system (Thermo Fisher Scientific, Austin, TX, USA) equipped with a NA-5MS column (60 m × 0.25 mm; 0.25 µm). The temperature settings for the oven were programmed as follows: an initial temperature of 50 °C was maintained for 2 min, followed by a heating rate of 5 °C min^{-1} until reaching 290 °C, where it was held for 10 min. Helium gas was used as the carrier gas, with a constant flow rate of 1 mL min^{-1}. The injector operated in split mode at a temperature of 280 °C, with an injection volume of 1 µL. The mass spectrometer was set to electron ionization mode with an energy of 70 eV, scanning the mass range from 40 to 550 Da. The interface temperature was maintained at 290 °C. The acquired data were processed using Chromeleon 7.2 software from Thermo Scientific (Sunnyvale, CA, USA). Compound identification was performed by comparing the obtained spectra with the NIST 2017 spectral library ver. 2.73 (Gaithersburg, MD, USA), considering only those species with a match higher than 75% with the library spectra.

2.2.6 HSQC

Spectra were recorded on a 600 MHz Bruker Avance III spectrometer equipped with an inversely detecting ^{1}H, ^{13}C, ^{15}N-triple-resonance cryogenically cooled TCI probehead. Processing of spectra was performed using the software Topspin 3.5. Analyses were performed using ~200.0 mg of the pyrolytic lignin samples dissolved in 800 µL deuterated methanol.

Proton pulse lengths were adjusted individually. The ^{1}H-^{13}C HSQC spectra were recorded with 2048 × 256 complex data points with spectral widths of 7.18 and 36.9 kHz (corresponding to acquisition times of 12.5 and 3.5 ms, respectively) accumulating 8 scans per t_1 increment and applying 16 dummy scans. A recycle delay of 2 s was used. Phase sensitivity in the indirect dimension was achieved by an echo/antiecho gradient scheme. To reduce artifacts TPPI was utilized with t_1 increments. Heteronuclear decoupling was achieved using GARP. The spectra were processed using a shifted quadratic sine-bell window-function.

2.2.7 Characterization of LMM and HMM at molecular-level by ultra-high-resolution mass spectrometry (UHRMS)

A Thermo Fisher Scientific Exactive Plus Orbitrap equipped with an Ion Max API source with an APCI probe was used for analyses. The LMM and HMM were dissolved in methanol (LC–MS grade, J.T. Baker) to obtain a solution with a concentration of 900 µg mL^{-1}. The stock solution was further mixed with 1000 µL of THF (LC–MS grade, J.T. Baker) to obtain the final sample with a concentration of 300 µg mL^{-1} (1:2—methanol/THF). The instrument conditions were set at sheath gas flow at 40 psi, auxiliary gas flow at 10 psi, ion source temperature at 300 °C, spray current at 4 µA, scanning range of 100–1000 Da, injection flow of 80 µL min^{-1}, and capillary temperature at 300 °C.

The determination of statistical values such as the number-average molecular mass (M_n) and the weight-average molecular mass (M_w) were calculated from Eqs. 1 and 2, respectively:

$$M_n = \frac{\sum_i M_i I_i}{\sum_i I_i} \tag{1}$$

$$M_w = \frac{\sum_i M_i^2 I_i}{\sum_i M_i I_i} \tag{2}$$

where M_i is the m/z value of peak i and I_i is the peak intensity [25]. Both parameters represent a weighted average of the molecular mass of the components, with M_w slightly overestimating the heavier ones.

Data processing was performed with Xcalibur 3.0 software (Thermo Scientific) and PetroMS 2.3.0 software (Petrobras, Rio de Janeiro, Brazil, and UNICAMP, São Paulo, Brazil), employing specific bio-oil composition assignment algorithms. For the elemental compositions that were observed concurrently within the sample and blank spectra, final intensities were determined as difference of sample and blank spectra intensities. Mass peaks relevant to isotopic distributions were identified and deleted. Criteria for the assignments of elemental compositions were tolerance error of ± 3 ppm, charge equals to − 1, and DBE less than 30. Regarding the elements, normal conditions for bio-oil

data ($CcHhNnOo$, $0 \le c \le 100$, $0 \le h \le 200$, and $0 \le o \le 15$) were used for these calculations [26]. Only ions with signal/noise ratio higher than 3 were analyzed.

Double-bond equivalence (DBE) values, which represent the number of rings plus the number of carbon double bonds in a given molecular formula, were calculated using the Eq. 3:

$$DBE = C - \left(\frac{H}{2} \right) + \left(\frac{N}{2} \right) + 1 \qquad (3)$$

Kendrick mass (KM), which effectively converts the mass of CH_2 from 14.01565 to exactly 14.00000, was calculated by Eq. 4:

$$\text{Kendrick mass} = \text{experimental mass} \times \left(\frac{14.00000}{14.01565} \right) \qquad (4)$$

The Kendrick mass defect (KMD), which represents the homologous series (namely, compounds with the same constitution of heteroatoms and number of rings plus double bonds, but different numbers of CH_2 groups), was calculated by the Eq. 5:

$$\text{KMD} = \text{round (Kendrick mass)} - \text{Kendrick Mass} \qquad (5)$$

3 Results and discussion

3.1 Extraction and fractionation of PyL

After separation the aqueous phase from the organic phase of the beech wood bio-oil the fractionation of the organic phase was performed, and the yields obtained in each solvent fractionation step are presented in Table 1.

The water content, determined by Karl Fischer technique, of 14.5 wt% present in the organic phase of BWBO corresponds to the water that is interacting with the organic molecules in the bio-oil through strong intermolecular interactions forming a single stable phase. The water content present in the organic phase varies from 15 wt% until a limit up of 30–50 wt% water, depending on the moisture of the starting biomass and the way of production and collection of the bio-oil [29].

Extractives are composed of fatty acids, fatty alcohols, terpenes, resin acids, and terpenoids, which have lower oxygen content than pyrolysis liquid compounds in general, and for this reason, the formation of an upper phase occurs that has a higher viscosity and heating value than the bottom phase. The phase separation was found to be enhanced by an increase in temperature and/or in storage time [21]. The organic phase was composed of 35.3 wt% of low molecular mass LMM lignin, a caramel-like product, and 11.05 wt% of high molecular mass HMM lignin, obtained as a fine powder, which was insoluble in DCM due its complex structure and high polymerization degree [18]. Solvent fractionation of PyL shows similar yields as those obtained by condensation and water precipitation of pyrolytic lignin from beech wood bio-oil, which returned 14.4% and 34% for PyL fractions with low and high molecular mass, respectively, according to Ruiz et al. [30]. Solvent fractionation of PyL shows different yields as those obtained by condensation and water precipitation which returned 14.4% and 34% for PyL fractions with low and high molecular mass, respectively, from beech wood bio-oil [25]. While compared to other studies that have isolated pyrolytic lignin from different bio-oils and fractionated it in LMM and HMM in Table 1, beech wood bio-oil showed higher yields of pyrolytic lignin, which was mainly composed of low molecular mass compounds. It has been proven that the origin of the biomass significantly affects the quantity of pyrolytic lignin present in bio-oils. Compared to other studies that have isolated pyrolytic lignin from different bio-oils and fractionated it in LMM and HMM, beech wood bio-oil showed higher yields of pyrolytic lignin, which was mainly composed of low molecular mass compounds.

3.2 Elemental characterization and higher heating value (HHV)

The elemental analysis results with the respective carbon (C), hydrogen (H), nitrogen (N), and oxygen (O) contents, beyond the higher heating values (HHV) for the BWBO, LMM, and HMM samples are presented in Table 2.

Table 1 Yields of organic phase fractionation

	BWBO organic phase (wt%)	Forest residues [27]	Pine wood [28]	Eucalyptus [28]
Water content	14.50	24.4	23.4–27.3	21.1
Solid	0.79	–	–	–
Extractives	9.79	–	–	–
Water solubles	28.57	56.5	41.7–43.6	51.9
LMM	35.30	14.5	18.6–20.1	15.7
HMM	11.05	4.6	12.4–12.9	11.3

Table 2 Elemental analysis of organic phase and pyrolytic lignin

Elemental composition (wt%) (wet basis)	PyL		BWBO	PyL from:		
	LMM	HMM	Organic phase	Beech wood [31]	Lauan sawdust [10]	Waste woods [32]
C	64.9	62.7	54.3	67.5	64.38	66.8
H	7.1	5.9	7.5	6.0	5.99	6.7
O*	28.0	31.0	38.2	26.3	29.55	26.0
N	< 0.2**	0.4	< 0.2**	< 0.2	0.08	0.5
O/C	0.32	0.37	0.53	0.29	0.34	0.29
H/C	1.31	1.13	1.66	1.07	1.12	1.20
HHV (MJ kg^{-1})	28.0	25.9	23.1	–	–	–

*Determined by difference; **below limit of quantification

The values of nitrogen content were negligible for all of lignin fractions, which is in accordance with the values obtained for wood-derived pyrolytic lignin [33]. Regarding hydrogen content, the HMM showed the lowest value. As for the carbon content of both fractions, LMM and HMM exhibited values 19.5% and 15.5% higher than those determined in BWBO, respectively. On the other hand, the oxygen content in LMM and HMM decreased when compared to BWBO, approximately 26.7% and 18.8% lower, respectively. This behavior results from the extraction process of the pyrolytic lignin. When water is used, the most polar compounds of the bio-oil, the most oxygenated ones, are extracted [34]. On the other hand, PyL is the non-water-soluble fraction due to its high degree of polymerization, resulting in a sample with a higher carbon content compared to the BWBO. Consequently, both fractions showed higher HHV compared to the original bio-oil. The LMM fraction showed the highest carbon content (approximately 65%) and HHV (28 MJ kg^{-1}), in agreement with results reported by Wang et al. [10]. The higher content of oxygen and hydrogen observed for the organic phase can be a result of the water content (14.5 wt%), as the results are given in wet basis. LMM and HMM elemental results are close with those of raw alkali lignin and it THF soluble

fraction, suggesting that HMM fraction is representative of the original lignin source in biomass [35].

3.3 Characterization of pyrolytic lignin samples by FTIR-ATR analysis

Based on the FTIR-ATR data (Fig. 1A and B), it is notable that beech wood PyL fractions (LMM and HMM) are composed of the same functional groups. However, they differ in absorption peak intensities. The main functional groups of pyrolytic lignin are observed to absorb in the wavenumber region at 1800–700 cm^{-1}. Hence, this spectral region was chosen as the fingerprint of the samples [10, 36].

In the fingerprint region of the samples, the peak that was absorb at 1705–1699 cm^{-1} corresponds to the non-conjugated C=O stretch vibration from ketone and ester groups. The presence of aromatic structures of the sample constituents resulted in the absorption peaks at 1602, 1515, and ~1430 cm^{-1} due to the aromatic ring vibration, and the peak at 1034 cm^{-1} is a result of the C–H deformation in plane of aromatic ring [10, 36]. The peaks at 1271 cm^{-1} and 1152 cm^{-1} correspond to C–O aromatic skeletal vibrations of guaiacyl (G) units [10], while the bands at 861 and 817 cm^{-1} were the results of C–H out-of-plane vibrations in

Fig. 1 FTIR-ATR (**A**) full spectra and (**B**) fingerprint region for pyrolytic lignin samples
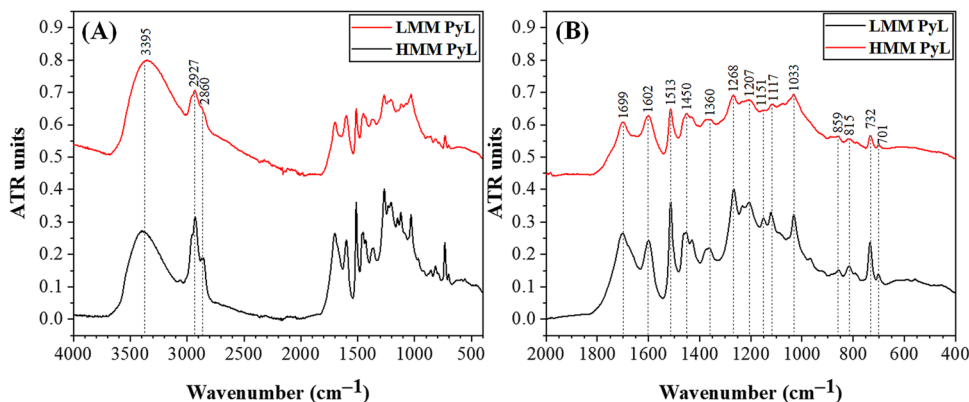
carbon positions 2, 5, and 6 of the guaiacyl (G) units [37], and at 1118 cm^{-1} corresponds to the aromatic C–H deformation in the syringyl (S) ring [10].

In addition, when considering the absorption region between 2900 and 3650 cm^{-1}, it is observed that the most intense band in the LMM sample is the broad band of ~3650–3100 cm^{-1}, corresponding to hydroxyl (O−H) stretch vibrations. On the other hand, in the HMM sample, the peaks at ~2930 and ~2850 cm^{-1}, which correspond to strong C−H (sp3) stretch absorptions, are higher [36]. This relationship between the strong C−H (sp3) stretch and the broad O−H stretch band suggests different scenarios for each fraction of pyrolytic lignin. In the LMM sample, the decrease in C−H stretching concurrent with an increase in O−H stretching vibrations indicates homolytic cleavage of the RC−OAr linkage in the aryl−O−alkyl ether bonds, resulting in the formation of phenoxy radicals [33]. Conversely, the preservation of these linkages leads to an increased C−H/O−H ratio, indicating a higher prevalence of non-fragmented oligomeric compounds. Therefore, LMM represents a product with a higher phenolic monomers content [36].

3.4 Molecular mass distribution of pyrolytic lignin fractions

The GPC plot with the results of molar distribution for the components in the LMM and HMM, as well as the respective average molecular mass (M_w), average molecular weights number (M_n), and the dispersity (D) values, is presented in Fig. 2. It is important to emphasize that due to the lignin aggregation phenomena as well as interaction between lignin and the solid support, GPC can be used only as a rough
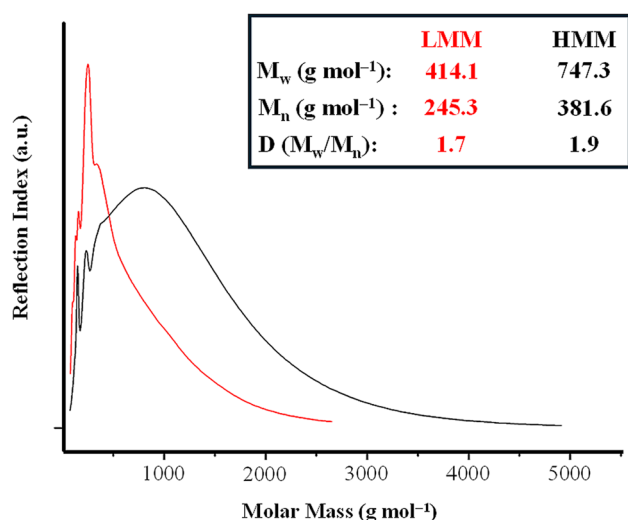

Fig. 2 Distribution of molecular mass by gel permeation chromatography (GPC)

indicator of M_w [38]. A method based in size exclusion chromatography was previously developed to quantification and characterization of the pyrolytic lignin from beech wood bio-oils. The condensation system and water precipitation method isolated two fractions of lignin with respective M_n of 580 and 890 Da, similar of the PL obtained in our work [30].

The M_w and M_n values in HMM are approximately 80% and 56%, respectively, higher than in LMM sample, which indicates a higher polymerization degree of the HMM constituents. In LMM sample, the M_w (414.1 g mol^{-1}) is in the range of molecular average mass corresponding to trimer compounds (319–477 g mol^{-1}), while the M_w in HMM sample (747.3 g mol^{-1}) is in the range attributed to pentamer compounds (637–763 g mol^{-1}) [39]. However, the range of the compounds present in the samples is larger than these two kinds of compounds. The more intense range in LMM, from approximately 250 to 500 g mol^{-1}, corresponds to dimers until tetramer compounds, and in HMM, the more intense range, from 500 to approximately 1200 g mol^{-1}, corresponds of tetramers until octamer compounds [39].

The M_w/M_n ratio, denominated as dispersity value (D), is used to determine the distribution of the molecular mass around the M_w value of compounds in the samples [40]. Despite the similar values, the D value of HMM (1.9) is higher than of the LMM sample (1.7), indicating the widest molecular weight distribution around the M_w for HMM. When compared to the D values reported by Leng et al. [18], for hardwood sawdust pyrolytic lignin that presented the same value of 1.47 for low LMM and high molecular mass HMM, and those reported by Ruiz et al. [30] for beech wood PyL (1.4 for both, low and high molecular mass), we can suggest that the precipitation parameters play an important role on the fractionation of different oligomeric structures of PyL.

3.5 Thermogravimetric behavior of LMM and HMM

Thermogravimetric analyses were carried out to evaluate the thermal decomposition profile of the low LMM and high molecular mass HMM pyrolytic lignin samples. The mass loss curves as a function of temperature (TG) and their respective derivative (DTG) are depicted in Fig. 3.

Comparing the TG curves of the samples, LMM sample exhibits a gradual thermal degradation profile in the temperature range from 60 to 500 °C (74.5% mass loss), characterized by at least four overlapping thermal decomposition events, as shown in the DTG curves, which may be associated with volatilization of low-mass monomers and degradation of oligomeric species [18]. In contrast, when analyzing the TG curve of the HMM sample, two clearly defined thermal degradation events were identified, occurring up to the temperature of 200 °C. The first event occurred in the range of 30 to 120 °C (2.9% mass
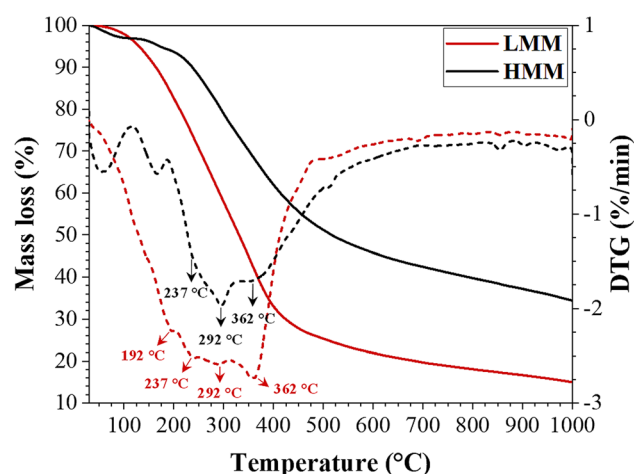
Fig. 3 Thermogravimetric behavior of low LMM and high molecular mass HMM pyrolytic lignin

loss) and was attributed to the evaporation process of the water adsorbed on the solid surface of the HMM. The second event, occurring between 120 and 200 °C (3.1% mass loss), was associated with the release of light volatile compounds. The main thermal degradation region, associated with the degradation of high molecular mass HMM oligomeric structures, occurred above 200 °C and extended up to 650 °C, being characterized by at least three overlapping thermal decomposition events [22]. At 1000 °C, the final residue from thermogravimetric analysis was 15.3% and 35% for LMM and HMM, respectively. The higher amount of residue in the HMM sample can be attributed to the higher rate of lignin repolymerization due to the presence of higher molecular mass oligomers in this sample, as observed in GPC analyses [41].

Evaluating the DTG curves, for both samples, the main mass loss region is composed of different overlapping degradation stages, which indicates that the thermal degradation process of pyrolytic lignin samples is highly complex and involves multiple reaction mechanisms [18]. The higher value of $DTG_{Máx}$ of the LMM sample (362 °C), the temperature with the highest rate of mass loss, indicates that it has greater thermal stability compared to HMM ($DTG_{Máx}$ 292 °C), which suggests a greater presence of C–C bonds, which require a higher temperature for its rupture due to its stability [36, 37], which is corroborated by the CHN data, in which the LMM sample has a higher C content than the HMM. After the $DTG_{Máx}$ value, both lignin samples degraded slowly over a wide temperature range compared to the main pyrolysis stage, due to the degradation of the carbonaceous residue forming after lignin polymerization and char formation during the main mass loss stage [37].

3.6 LMM and HMM GC/MS analysis

On account of the observed mass loss in the thermogravimetric (TG) analyses starting at 100 °C, both fractions underwent GC/MS analysis to assess the presence of volatile compounds. Notable disparities were observed in the chromatographic profiles of the LMM and HMM samples, which are available in Fig. S1 of the supplementary material. The LMM sample exhibited a uniform distribution of compounds with comparable intensities, resulting in a homogeneous chromatogram. Conversely, the HMM sample revealed the presence of four prominent peaks, while the remaining peaks exhibited significantly lower concentrations. Subsequent integration and compound identification led to the characterization of approximately 80% and 84% of the total area of the LMM and HMM chromatograms, respectively, in the GC/MS analysis.

The identified compounds were grouped into three main chemical classes: phenolic monomers, sugar derivatives, and carboxylic acids (in which the presence of short-chain acids and lipid acids was observed). The list of identified compounds, sorted according to their respective class, is presented in Table 3.

Considering the pyrolysis process of beech wood biomass, which produced the bio-oil used in the isolation of pyrolytic lignin in this study, it is assumed that all thermolabile structures at the GC/MS working temperature (300 °C) were volatilized. Therefore, the mass loss observed in the TG (approximately 36% and 16% of the total mass in the LMM and HMM samples, respectively) up to this temperature was chemically characterized using the GC/MS technique. It is important to note that the derivatization process, prior to the GC/MS analysis, reduces the polarity of the molecules, resulting in a decrease in the required volatilization temperature [42]. Thus, it is plausible to assert that an even higher percentage of the lignin fractions may have been successfully characterized, with the aforementioned percentages being the minimum values achieved under the specified experimental conditions.

Regarding the chemical class of representative compounds, it was found that the LMM primarily consists of phenolic compounds, constituting approximately 53% of the total area, with 2-methoxy-4-methylphenol being the most abundant compound, accounting for 13.1% of the total area in the chromatogram. Additionally, the increasing amount of guaiacol, 2-methoxy-4-methylphenol, and isoeugenol (E) has direct correlation with the pyrolysis process temperature suggesting in our case that the biomass was submitted up to 525 °C [35]. In contrast, the HMM predominantly comprises of carbohydrate derivatives, covering approximately 56% of the volatile fraction, which can contribute to the intense broadband at 3406 cm^{-1} in FTIR spectra. Among these derivatives, 2-deoxy-beta-D-ribopyranose (26.9%) and

Compound	Ret. time (min)	Precursor units	LMM (%)	HMM (%)	Py-HMM (%)
Total phenolic monomers			53.3	21.7	55.9
Phenol	15.97	H	0.5	–	0.9
Alkylphenols			*3.1*	*1.1*	*2.6*
o-Cresol	18.42	G	0.8	–	0.6
m-Cresol	18.73	G	0.5	–	0.4
p-Cresol	19.07	H	1.4	1.1	0.5
2,4-Dimethylphenol	20.88	G	–	–	0.2
2,3-Dimethylphenol	21.34	G	–	–	0.4
3-Ethylphenol	21.66	G	0.4	–	0.3
Chavicol	26.60	H	–	–	0.2
Methoxyphenols			*42.0*	*13.0*	*22.6*
Guaiacol	21.32	G	6.9	–	8.0
2-Methoxy-3-methylphenol	23.69	G	–	–	0.6
2-Methoxy-4-methylphenol	23.89	G	13.1	3.1	6.4
2,3-Dimethoxyphenol	26.26	S	–	–	0.3
Eugenol	28.00	G	5.5	–	–
Isoeugenol, (E)-isomer	29.29	G	3.4	–	0.8
Vanillin	29.81	G	3.1	1.5	2.5
Isoeugenol, (Z)-isomer	30.51	G	3.0	1.8	3.1
Acetoisovanillone	31.79	G	2.3	4.5	0.3
3-Vanilpropanol	35.93	G	1.4	2.1	0.7
Coniferyl aldehyde	36.84	G	3.2	–	–
Hydroxyphenols			*7.7*	*7.5*	*29.9*
Catechol	23.75	G	3.0	2.8	11.6
3-Methylcatechol	25.71	G	2.5	1.8	7.7
4-Methylcatechol	26.09	G	–	–	3.1
Hydroquinone	26.12	G	–	–	0.8
3,4-Dihydroxybenzaldehyde	27.54	G	1.6	2.9	2.6
Methylhydroquinone	27.66	G	–	–	0.5
3,5-Dihydroxybenzaldehyde	27.69	G	–	–	2.6
Hydroxychavicol	29.43	G	0.7	–	0.9
Total Sugar Derivatives			***8.6***	***55.8***	***17.6***
1,4-Dioxane-2,5-diol	22.76	C	–	–	0.3
Maltol	23.22	C	–	–	0.2
2-Deoxy-alpha-D-ribopyranose	31.01	C	1.0	1.6	1.3
2-Deoxy-beta-D-ribopyranose	31.66	C	5.8	26.9	14.6
isomer of Levoglucosan	32.83	C	0.9	7.5	0.7
Levoglucosan	33.26	C	0.9	16.4	0.5
Methyl a-Arabinofuranoside	31.41	C	–	2.3	–
A-Arabinofuranose	32.31	C	–	1.1	–
Acids			***17.9***	***6.8***	***0.0***
Glycolic acid	16.47	–	1.2	4.7	–
Octanoic acid	22.29	–	0.6	–	–
Butanedioic acid	23.64	–	1.0	1.0	–
Butanedioic acid, methylene	24.59	–	–	1.1	–
Palmitic Acid	40.51	–	1.5	–	–
9-Octadecenoic acid, (E)-	43.67	–	1.7	–	–
Stearic acid	44.10	–	0.6	–	–
Pimaric acid	45.59	–	0.6	–	–
Isopimaric acid	46.19	–	0.8	–	–
Dehydroabietic acid	46.92	–	5.0	–	–

Table 3 Identified volatile compounds presents in LMM and HMM fractions

Compound	Ret. time (min)	Precursor units	LMM (%)	HMM (%)	Py-HMM (%)
Total phenolic monomers			53.3	21.7	55.9
7-Oxodehydroabietic acid	50.30	–	5.0	–	–
Unknows			*20.1*	*15.8*	*26.5*

Table 3 (continued)

levoglucosan (16.4%) are the most prominent compounds within this class. The derivatization of HMM fraction to GC/MS analysis allows to identify the sugar derivatives improving the overview of the chemical constituents in comparison with direct analysis of dichloromethane insoluble fraction of pyrolysis oil [43]. It is noteworthy that the presence of a significant quantity of volatile or low molecular mass compounds in the samples, even after the isolation process of lignin, can be attributed to the strong intermolecular interactions between the compounds present in the bio-oil and the pyrolytic lignin structures [18]. The results of the GC/MS analysis corroborate with the data obtained by TG and help to explain why LMM begins to lose mass approximately 100 °C before HMM, since, in general, phenolic monomers are more volatile than sugar derivatives.

Concerning the chemical composition dissimilarity observed in the compounds identified by GC/MS in the two lignin fractions, the polarity of dichloromethane (DCM) facilitated the extraction of phenolic compounds, leading to their enrichment in the fraction soluble in DCM, namely the low molecular mass LMM pyrolytic lignin. Conversely, the fraction insoluble in DCM, corresponding to the high molecular mass HMM pyrolytic lignin, predominantly retained derivatives of free sugars. This partition phenomenon resulted in the segregation of phenolic compounds in LMM and the retention of sugar derivatives in HMM.

In view of the greater degree of polymerization of HMM compared to LMM, the high molecular mass fraction was subjected to the analytical procedure of Py(offline)-GC/MS to identify the main constituent units of the HMM pyrolytic lignin. The offline pyrolysis yielded a solid product with a yield of 54%, consistent with the thermogravimetric (TG) mass loss at 500 °C. Additionally, approximately 33% of the HMM fraction was converted into total liquid products, which were subsequently subjected to GC/MS analysis. Around 74% of the total chromatogram area of the HMM pyrolytic product (Py-HMM) was successfully characterized. The compositional analysis revealed that the pyrolytic product derived from the high molecular mass (HMM) fraction exhibited a composition consisting of approximately 56% phenolic monomers, derived from lignin, and approximately 18% sugar-like compounds. These proportions indicate that after the pyrolysis process, the content of phenolic monomers, compared to the original HMM sample, is increased by approximately 34% points, while the content of sugar derivatives reduces by

~38% points. Notably, despite a significant reduction in the content of sugar-like compounds, the presence of approximately 15% of 2-deoxy-beta-D-ribopyranose was observed in the pyrolytic product (Py-HMM), suggesting that a portion of this carbohydrate remained chemically bound to lignin, since the lignin is chemically linked to polysaccharides in wood [44].

Regarding the phenolic monomers, a noticeable increase was observed, with the area of methoxyphenols showing a relative increase of about 74% and the area of alkylphenols exhibiting an approximate increase of 300%. Among the methoxyphenols, guaiacol emerged as the major compound, constituting 8% of the total area percentage, which was not detected in the original HMM fraction before pyrolysis. The second most prominent methoxyphenol compound was 2-methoxy-4-methylphenol, accounting for 6.4% of the total area. Among the hydroxyphenols, catechol and 3-methyl-catechol were the predominant compounds, representing 11.6% and 7.7% of the total area of the total ion current chromatogram (TICC), respectively. The pyrolysis products of HMM were classified as hydroxyphenyl (H), guaiacyl (G), and syringyl (S) type, for the lignin derivatives, in addition to carbohydrate derivatives (C). Overall, 54% by area of phenolic monomers produced in the HMM pyrolysis is derived from guaiacyl units, 1.6% derived from hydroxyphenyl units, and 0.3% of products derived from the degradation of syringyl units. The predominance of guaiacyl units in the structure of pyrolytic lignin derived from beech wood bio-oil is consistent with the results found by Scholze et al. [45].

The distribution of lignin fragments in terms of guaiacyl, hydroxyphenyl, and syringyl units was analyzed, revealing percentages of 96.6%, 2.9%, and 0.5%, respectively. These findings are consistent with previous research conducted by Scholze et al. [45] on pyrolytic lignin derived from softwood mixture and pine, which also showed higher levels of guaiacyl unit derivatives at 94% and 95.6%, respectively. The calculated S/G ratio, based on the contents of guaiacyl and syringyl derivatives, was found to be less than 0.01. This value is comparable to results obtained by Laskar et al. [46] for water-only samples of pretreated Miscanthus (0.13) and Scholze and Meier [47] for pyrolytic lignins from mixed softwood (0.00) and pine (0.03). In contrast, eucalyptus kraft lignin exhibited a higher S/G ratio ranging from 0.89 to 1.21 [48]. The lower S/G ratio indicates greater difficulty in delignification due to the presence of 5–5′ bonds between the lignin guaiacyl units [49].

3.7 HSQC

The HSQC NMR technique is a useful tool for the characterization of complex samples, as it can resolve overlapping resonances observed in 1D ^1H or ^{13}C NMR spectra due to the considerable spectrum data scatter provided by 2D NMR methods, obtaining a good resolution of the key resonances of the sample components, which allows an interpretation of a significant amount of the data obtained [50, 51]. To get further information about the structure of the LMM and HMM pyrolytic lignin samples, a 2D HSQC NMR was performed and the spectra are shown in Fig. 4.

From the HSQC NMR spectra for pyrolytic lignin, the presence of four different regions according to the chemical shift (δ) for H and C was determined, whether it was LMM or HMM. These regions are the aromatic region (δC/δH 95–145/6–8.25 ppm), aliphatic C−O region (δC/δH 50–95/2.75–6.0 ppm), aliphatic C−C region (δC/δH 5–50/0.5–3.0 ppm), and polysaccharide anomeric region (δC/δH 90–110/3.5–6.0 ppm). In the spectra of the LMM and HMM samples, Fig. 4, respectively, highlights the main regions of component distribution. The same regions of resonance distribution, as well as some common correlation peaks, were observed in both spectra. The intense correlation signal at δC/δH ~56.3/3.80 corresponds to the methoxyl groups [10, 52], while the prominent correlation peaks in the aromatic's region at δ_C/δ_H 113/6.7, 115.7/6.7, and 121/6.5 can be attributed to C_2/H_2, C_5/H_5, and C_6/H_6 correlations, respectively, of guaiacyl units (C−H) and ferulate (C−H) [53], evidencing that both low LMM and high molecular mass HMM pyrolytic lignins are mainly composed of guaiacyl units. This result corroborates the observed by the analysis of HMM by Py-GC/MS.

It should be considered that lignin is a complex macromolecule constituted mainly from two primary precursors, coniferyl and sinapyl alcohols, in addition to small amounts of p-coumaryl alcohol. The lignin monomers, derived from aromatic alcohols, are connected by means of C−C and C−O−C bonds, such as β-5, 5–5, β-β, β-O-4, and 4-O-5. These bonds give rise to substructures such as phenylcoumaran, biphenyl, resinol, alkyl-aryl ether, and biphenyl ether. However, it is worth noting that the predominant β-aryl ether units in lignin involve βO-4 bonds [54]. Thus, it is possible to notice that the HMM sample presented greater amounts of correlation peaks in the aliphatic C−O region (pyrolytic sugars). These correlation peaks indicate the existence of various interunit linkages; i.e., the signals at δ_C 65–90 ppm are correlated with the alkyl−O−aryl, a−O−aryl, and c−O−Alkyl γ-ether bonds, and the peaks at 4.5–4.2 ppm refer to the presence of benzyl alcohol structures in the high molecular weight mass pyrolytic lignin [55]. This indicates that the HMM sample has a higher degree of polymerization than the LMM, which does not show signs in this region, which is corroborated by the GPC data.

Finally, some signals at δC/δH 60–100/3.0–5.0 ppm were assigned to pyrolytic sugars. Most pyrolytic sugars were effectively removed during the separation of bio-oil through water extraction. However, due to intermolecular interactions between sugars and pyrolytic lignins, a small quantity of sugars remained in the water-insoluble phase even after extraction with a minimal amount of water. Therefore, the sugar structures present in the HMM fraction can be associated with lignin oligomer structures (mainly guaiacyl structures, possibly through ferulate ester linkages) and/or residual amounts of sugars (monomers
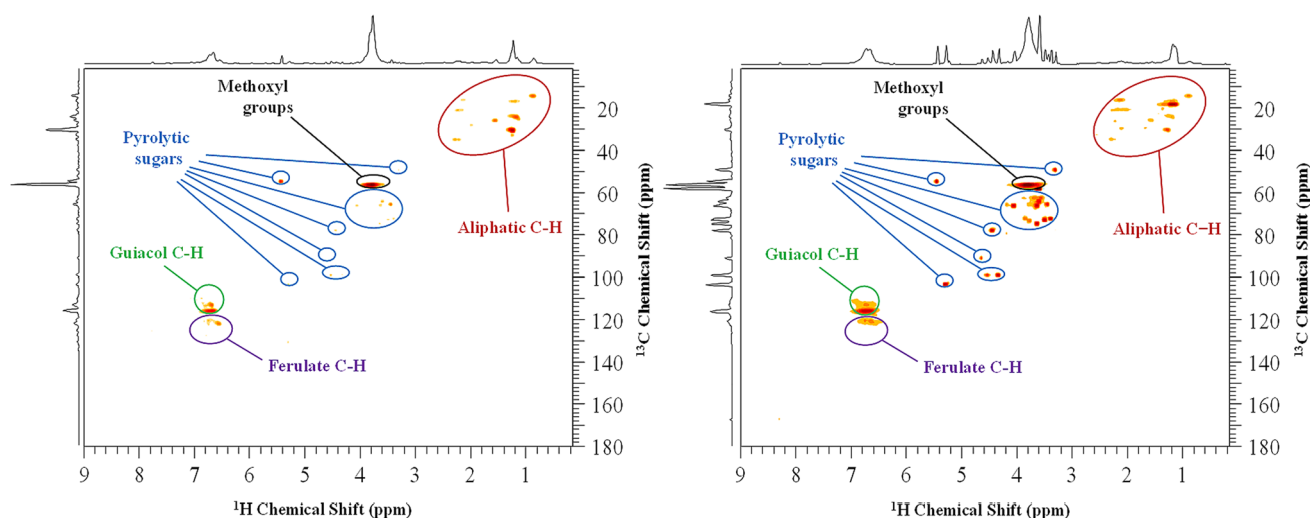

Fig. 4 HSQC spectra of the pyrolytic lignin fractions highlighting the aliphatic C–H, aliphatic C–O (pyrolytic sugars and methoxyl groups) and aromatic regions (guaiacol and ferulate). LMM, left side; HMM, right side

structures). These data are also consistent with the analysis of HMM sample by Py-GC/MS and elemental analysis.

3.8 Evaluation of the molecular distribution of chemical constituents of LMM and HMM pyrolytic lignin by APCI(−)-FT Orbitrap MS

The APCI(−)-Orbitrap MS data (see Fig. 5) were used for a more comprehensive understanding of the types of compounds, their molecular formulas, chemical classes, and potential base structures present in both fractions of pyrolytic lignin.

The differences in the profile of LMM and HMM fractions were notably visible. In the LMM sample, ions within the m/z range of 100 to approximately 700 were observed, whereas in the HMM the range extend to m/z 800. Furthermore, the ion distribution shows that molecular ions with m/z values greater than 300 are more intense in the HMM fraction. This distinguished distribution had an important effect on profiles of mass spectrum, in which the LMM fraction showed lower values of M_n and M_w (322.22 and 357.51, respectively) than the HMM fraction (M_n and M_w equals to 347.04 and 395.44, respectively). This trend is in accordance with the of M_n and M_w values obtained by GPC for these samples.

Considering the total-ion current, an amount of 8544 and 10,302 was detected in the LMM and HMM fractions, respectively. For the molecular characterization, only ions with signal-to-noise ratio above 3 were considered for data treatment, which accounted for 2509 and 2773 ions for LMM and HMM, respectively. Since molecules with acidic characteristics, i.e., oxygenated compounds, are preferentially ionized in the negative mode of analysis, and also taking into account the low nitrogen content in the samples (less than 0.4%), the processing conditions were tailored to focus solely on compounds falling within the O_x class (where x ranges from 1 to 15). Thus, approximately 74% and 66% of the molecules with S/$N > 3$ had their chemical formula attributed.

The characterized ions were sorted into different chemical classes according to the number of heteroatoms present in their molecular formulas (see Fig. S2). Regarding the chemical classes identified in the samples, it was observed that either in terms of absolute number of molecules or relative intensity, the HMM has a greater abundance of more oxygenated compounds, mainly in classes O_9 to O_{15}. In contrast, compounds with a lower number of oxygens per structure, from O_2 to O_6, are more abundant in low molecular mass-LMM pyrolytic lignin. To promote a greater understanding of the chemical composition of the pyrolytic lignin fractions, the UHRMS data were plotted on graphs commonly used for molecular characterization, such as oxygen number vs. carbon number, Kendrick diagrams, DBE vs. carbon number graphs, and van Krevelen diagrams, which promote a more comprehensive assessment of the distribution of compounds (see Fig. 6).

The molecular distribution of ions for evaluation of oxygenation degree, as depicted in Fig. 6A, where the carbon number (C_n) is plotted against the oxygen number (O_n), demonstrated dissimilarities between the samples. Despite
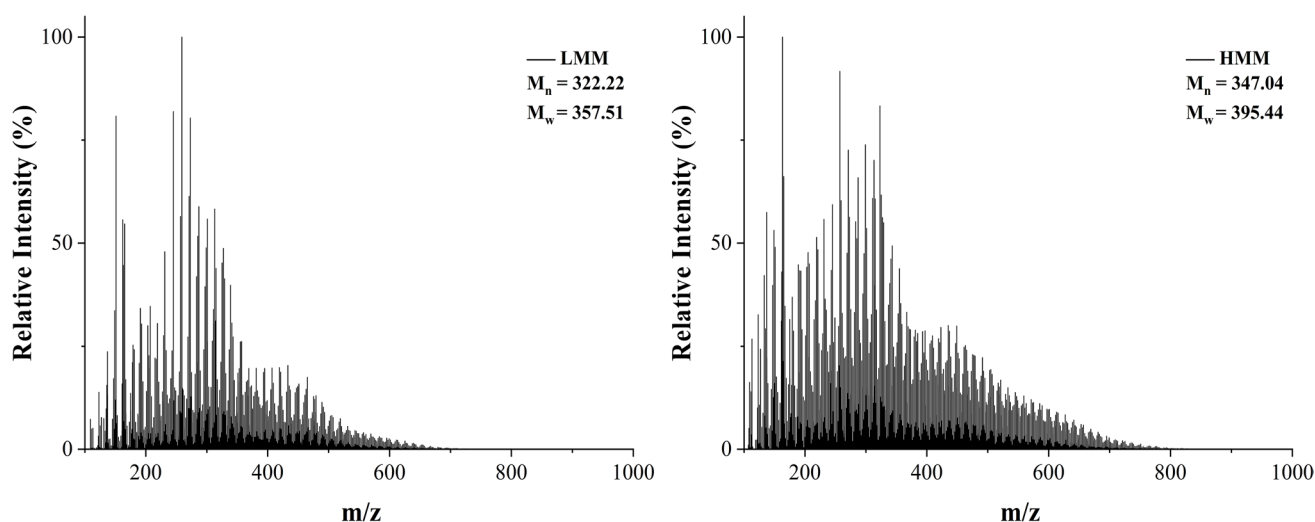

Fig. 5 Mass spectra obtained by APCI(−)-FT-Orbitrap MS for the LMM and HMM pyrolytic lignins. For each spectrum, the values of the weight-average molecular mass (M_w) and the number-average molecular mass (M_n) are described

both fractions having the same range on the carbon number axis, the low molecular mass (LMM) sample exhibited ions with up to 11 oxygen atoms, whereas the high molecular mass (HMM) fraction extended this range up to O_{12}. When analyzing the total molecular distribution, the compounds in both HMM and LMM showed similar overall distributions. However, a remarkable distinction was observed when considering the most intense compounds (with a relative intensity $\geq 10\%$). The HMM fraction displayed a broader region compared to the LMM, where the ions were distributed in C_n ranging from 5 to 36 and O_n ranging from 3 to 10. On the other hand, in the LMM fraction, the distribution was confined to a C_n region between 5 and 30 and O_n between 2 and 7. This observation indicated a higher abundance of larger and more functionally complex phenolic oligomers within the high molecular mass pyrolytic lignin fraction.

Despite the high presence of carbohydrate derivatives in the HMM sample, as seen in the GC/MS and HSQC analyses, the graph of carbon number vs. DBE (Fig. 6B) corroborated this proposition. Since the number of carbons increased, there was also an increase in the degree of unsaturation of these ions.

In the van Krevelen diagrams of the samples (Fig. 6C), it was observed that in the LMM fraction, the ions were distributed in three main regions, which correspond to compounds belonging to the class of lipid-like compounds (region delimited in yellow), sugar-like compounds (region delimited in red), composed of carbohydrates and dehydrocarbohydrates, and lignin derivatives (region delimited in black) [56]. While in the HMM, the ions were distributed in two regions, referring to sugar-like compounds and lignin derivatives, the latter being the region with the

Fig. 6 Compositional characterization of LMM and HMM pyrolytic lignins from BWBO. **A** Diagrams of oxygen number versus carbon number; **B** diagrams of DBE versus carbon number; and **C** diagrams of van Krevelen for LMM and HMM
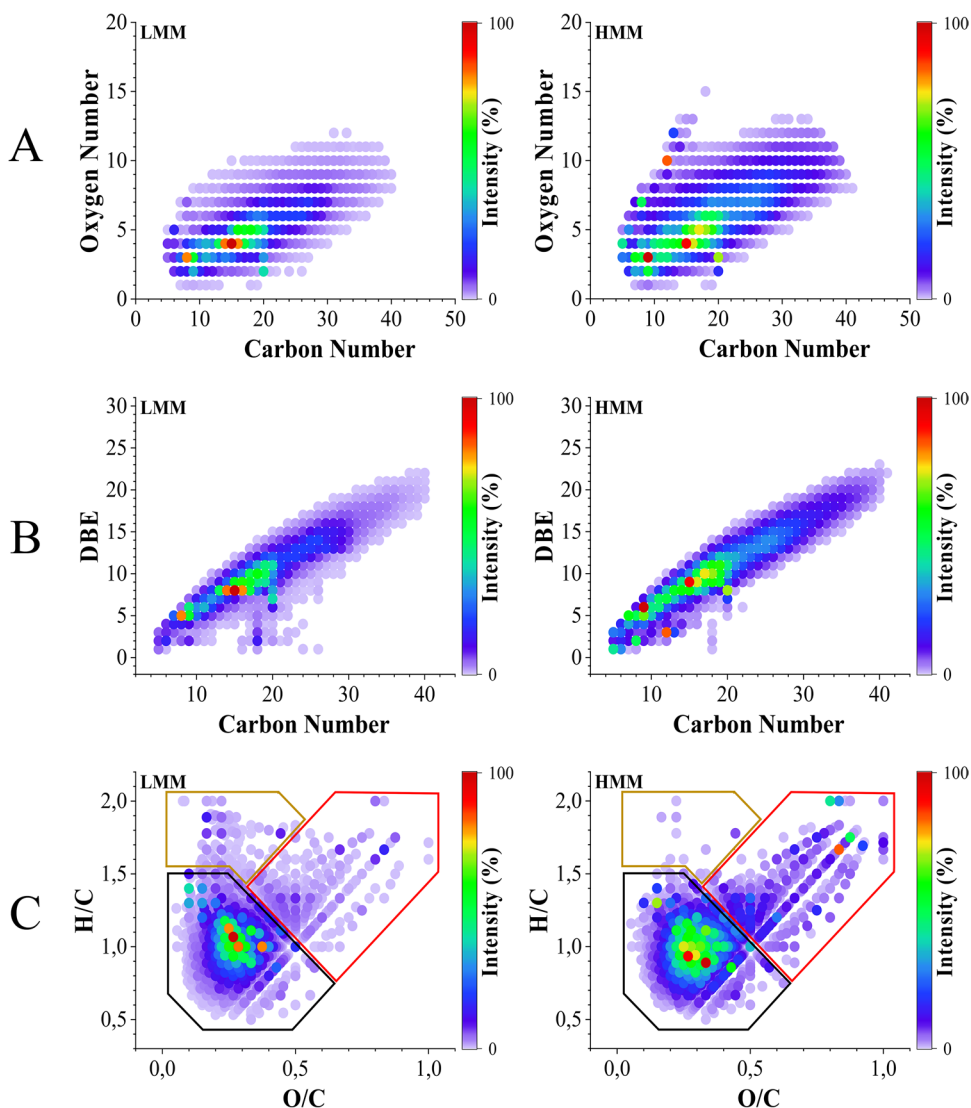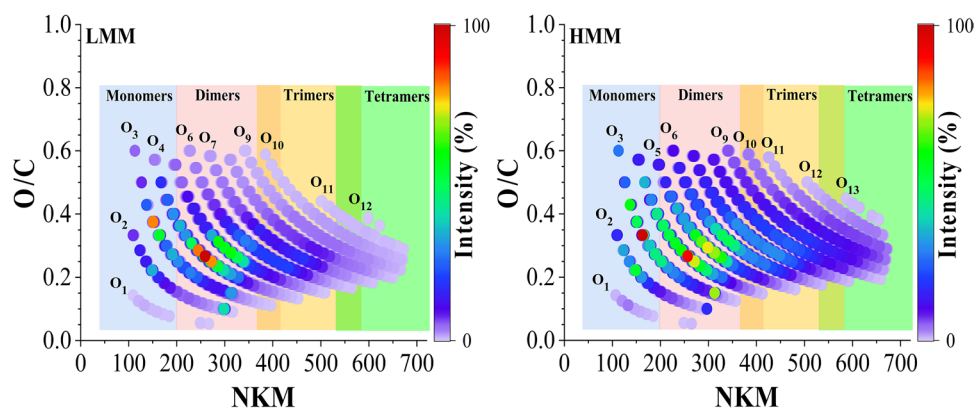
Fig. 7 Diagrams of Kendrick mass defect vs. O/C plot for LMM and HMM pyrolytic lignin of BWBO obtained by fast pyrolysis, with highlighted regions of the main-lignin compounds

greatest abundance of ions, mainly in the high molecular mass pyrolytic lignin sample. Due to the clustering of all ions associated with lignin-derived compounds within a single region in the van Krevelen diagram, conducting a more thorough analysis of compounds within this class posed challenges. To overcome this limitation and gain deeper insights into the lignin-derived compounds, a Kendrick mass defect vs. O/C plot was utilized, focusing on these ions, as illustrated in Fig. 7. This analytical approach enabled a more effective examination of the compounds derived from lignin, providing valuable information for further investigations.

The compounds in the phenolic region of the van Krevelen diagram (see Fig. 6C) exhibit a nominal mass range of 100 to ~700 Da. Based on their mass range, these ions have been classified into monomers (100 to 250 Da), dimers (250 to 450 Da), trimers (400 to 600 Da), and tetramers (550 to 750 Da) of guaiacyl subunits. These ranges were calculated using the results from the GC/MS analysis of the pyrolytic lignin fractions, as well as subsequent Py-offline-GC/MS analysis of the HMM fraction, which indicated that the pyrolytic lignin mainly comprises guaiacyl-derived subunits (with identified monomers falling within the molecular mass range of 108 to 182 g mol^{-1}). Furthermore, it is noted that these subunits can polymerize into a multitude of molecular arrangements beyond the typical alkyl−O−aryl linkages.

Our interpretation also was supported by the results presented to pyrolytic lignin isolated from hybrid poplar milled wood pyrolyzed at 500 °C and characterized by ESI-FT-ICR MS. In this case, the UHRMS analyses presented compounds with $1000 > m/z > 500$ distributing the pyrolysis oligomers in trimers ($C_{28}H_{28}O_9$ m/z 508 to $C_{33}H_{40}O_{12}$ m/z 628) and tetramers ($C_{37}H_{38}O_{12}$ m/z 674 to $C_{40}H_{44}O_{14}$ m/z 748) with few variations on the limits considering the

pyrolysis parameters employed. The work presented proposed assignment of oligomer structures were based on the combination of monomer unit of *p*-hydroxyphenyl, guaiacyl, and syringyl as well as the estimation of normal boiling point for the oligomers [57]. These proposed ranges of oligomeric compounds align with the dimer and trimer ranges (316 to 436 Da and 519 to 639 Da, respectively) identified by Asare et al. [58], who determined oligomeric structures of synthetic lignin ionized in [M + Li]$^+$ form and fragmented through high-energy collisional dissociation. Additionally, Prothmann et al. [59] identified dimers with masses ranging from 243 to 395 Da, trimers from 395 to 509 Da, and tetramers with masses of 627 to 631 Da in kraft lignin using UHPLC/HRMSn.

Furthermore, the NKM vs. O/C graph provides new insights not only into the degree of polymerization of pyrolytic lignin constituents but also into the chemical class to which each ion belongs. It reveals a well-defined decreasing trendline for each O$_n$ value. Consequently, it can be affirmed that the composition of the HMM fraction, concerning phenolic derivatives originating from the lignin portion of beech wood bio-oil obtained through rapid pyrolysis, exhibits a higher abundance of guaiacyl dimers, trimers, and tetramers compared to the LMM fraction, primarily belonging to O$_4$ to O$_{10}$ classes, distributed within a carbon number range of 13 to 40 and a DBE range of 8 to 23.

4 Conclusions

This work presented a comprehensive characterization of the pyrolytic lignin obtained from beech wood bio-oil, focusing on the low (LMM) and high molecular mass (HMM) fractions, 414 g mol^{-1} and 747 g mol^{-1} determined by GPC analysis, respectively. The results showed

that pyrolytic lignin accounted for 46.35% m/m of beech wood bio-oil, which is mostly composed of LMM (~76% m/m pyrolytic lignin), whereas HMM fraction accounted for ~33% m/m of the pyrolytic lignin in BWBO. Compared to BWBO (H/C = 1.66; O/C = 0.53), the LMM and HMM fractions have lower H/C (1.31 and 1.13, respectively) and O/C (0.32 and 0.37, respectively) ratios, which indicates a greater predominance of aromatic and less oxygenated structures. FTIR analysis confirmed the greater presence of aromatic structures in both fractions, with greater intensity in the region attributed to the guaiacyl units. TG revealed different thermal degradation profiles for LMM and HMM, from which it was possible to see that the HMM sample has greater thermal stability, due to its greater degree of oligomerization. This was confirmed by HSQC and Py-GC/MS analysis. In addition, Py-GC/MS revealed that HMM showed an increased presence of phenolic monomers, particularly guaiacyl-derived units (54% in relative area), resulting from the degradation of the oligomers present in the sample. Despite the isolation of pyrolytic lignin, GC/MS analysis revealed the presence of sugar derivatives and carboxylic acids in both fractions, the result of strong intermolecular interactions between bio-oil compounds and lignin. The HMM fraction, in terms of phenolic derivatives, shows a greater abundance of guaiacyl dimers, trimers, and tetramers compared to the LMM fraction. From the results presented, it can be concluded that, from an analytical point of view, proposing UHRMS for the characterization of pyrolytic lignin facilitates an accurate understanding of the composition of the product, as well as the process. Furthermore, from an economic point of view, the BWBO LMM fraction can be used as an alternative source of phenolic monomers due to the higher concentration of these compounds (~53% in area by GC/MS) in this fraction. With regard to HMM, due to its higher degree of polymerization, it is necessary to use depolymerization techniques to further produce phenolic monomers. Future work should therefore focus on optimizing and upscaling the pyrolytic lignin extraction process, bearing in mind environmental and economic aspects, as well as investigating the chemical stability of these fractions and studying the conversion and/or integration of pyrolytic lignin into chemical products. In conclusion, this work presented a comprehensive characterization of pyrolytic lignin obtained from beech wood bio-oil, with a focus on the low molecular mass (LMM) and high molecular mass (HMM) fractions. The lignin samples were subjected to an array of analytical techniques, including FTIR, GPC, TG, GC/MS, multidimensional NMR spectroscopy, and high-resolution mass spectrometry (UHRMS). Elemental analysis revealed higher carbon content and lower oxygen content in both

fractions, leading to elevated heating values compared to the original bio-oil. FTIR analysis indicated the presence of aromatic structures, as well as higher intensity in the region attributed to guaiacyl units and lower absorption intensities in the region attributed to syringyl units in the lignin frac-tions. GPC analysis demonstrated a higher degree of polym-erization in the HMM fraction. The TG revealed different profiles of thermal degradation for LMM and HMM, from which it was possible to visualize that the HMM sample presents higher thermal stability. Despite the isolation of pyrolytic lignin, the GC/MS analysis identified the presence of phenolic monomers, sugar derivatives, and carboxylic acids in both fractions, the result of strong intermolecular interactions between the bio-oil compounds with lignin, with the HMM fraction exhibiting a greater abundance of sugar-like compounds due to lignin fractionation in LMM and HMM with DCM. Py-GC/MS analysis of HMM revealed an increased presence of phenolic monomers, particularly guaiacyl units, resulting from the degradation of oligom-ers present in the sample. HSQC NMR spectra confirmed the presence of guaiacyl units and phenolic compounds in both fractions, with HMM showing a higher degree of polymerization and a broader range of compounds. Mass spectrometry analysis highlighted the distinct molecular distributions in HMM and LMM, with the former contain-ing a higher abundance of oxygenated compounds. Together with the previous data, it was possible to determine that the polar composition of the HMM fraction, in terms of phe-nolic derivatives, exhibits a higher abundance of guaiacyl dimers, trimers, and tetramers compared to the LMM frac-tion. These findings contribute to an improved understanding of the structure and composition of pyrolytic lignin and have significant implications for its potential applications in the biofuels, chemicals, and materials industries. Furthermore, the use of UHRMS has been proposed for the determina-tion of the composition of pyrolytic lignin, considering the monomers and oligomers present in each fraction.

Author contribution W.R.S. instrumental analysis, interpretation of results, writing—original draft; T.M.S. developed the method for UHRMS analysis, data interpretation, writing—original draft; J.C.C. instrumental analysis, interpretation of the UHRMS results,

writing—original draft; C.C.S. investigation, interpretation of results, critical revision of the manuscript; K.R. project coordinator, conceptualization, final revision of the manuscript; N.D. conceptualization, final revision of the manuscript; A.W.J. project coordinator, resources, conceived and designed the analyses, data analysis, final revision of the manuscript. All authors have read and agreed to the published version of the manuscript.

Data availability Supplementary information is available.

Declarations

Ethical approval Not applicable

Competing interests The authors declare no competing interests.

References

1. Figueirêdo MB, Hita I, Deuss PJ et al (2022) Pyrolytic lignin: a promising biorefinery feedstock for the production of fuels and valuable chemicals. Green Chem 24:4680–4702. https://doi.org/10.1039/D2GC00302C
2. Yin W, Alekseeva MV, Venderbosch RH et al (2020) Catalytic hydrotreatment of the pyrolytic sugar and pyrolytic lignin fractions of fast pyrolysis liquids using nickel based catalysts. Energies 13:285. https://doi.org/10.3390/en13010285
3. Brethauer S, Shahab RL, Studer MH (2020) Impacts of biofilms on the conversion of cellulose. Appl Microbiol Biotechnol 104:5201–5212. https://doi.org/10.1007/s00253-020-10595-y
4. Guedes RE, Luna AS, Torres AR (2018) Operating parameters for bio-oil production in biomass pyrolysis: a review. J Anal Appl Pyrol 129:134–149. https://doi.org/10.1016/J.JAAP.2017.11.019
5. Karagoz P, Bill RM, Ozkan M (2019) Lignocellulosic ethanol production: evaluation of new approaches, cell immobilization and reactor configurations. Renewable Energy 143:741–752. https://doi.org/10.1016/j.renene.2019.05.045
6. Yang Y, Xu X, He H et al (2023) The catalytic hydrodeoxygenation of bio-oil for upgradation from lignocellulosic biomass. Int J Biol Macromol 242:124773. https://doi.org/10.1016/j.ijbiomac.2023.124773
7. Waters CL, Janupala RR, Mallinson RG, Lobban LL (2017) Staged thermal fractionation for segregation of lignin and cellulose pyrolysis products: an experimental study of residence time and temperature effects. J Anal Appl Pyrol 126:380–389. https://doi.org/10.1016/j.jaap.2017.05.008
8. Manrique R, Terrell E, Kostetskyy P et al (2023) Elucidating biomass-derived pyrolytic lignin structures from demethylation reactions through density functional theory calculations. Energy Fuels 37:5189–5205. https://doi.org/10.1021/acs.energyfuels.2c04292
9. Wang J, Minami E, Kawamoto H (2023) Role of pyrolysis in pyrolysis-assisted catalytic hydrogenolysis of lignin and mechanistic insights into catalytic conversion. J Anal Appl Pyrol 170:105930. https://doi.org/10.1016/j.jaap.2023.105930
10. Wang Y, Wang S, Leng F et al (2015) Separation and characterization of pyrolytic lignins from the heavy fraction of bio-oil by molecular distillation. Sep Purif Technol 152:123–132. https://doi.org/10.1016/j.seppur.2015.08.011
11. Zhang L, Zhang S, Hu X, Gholizadeh M (2021) Progress in application of the pyrolytic lignin from pyrolysis of biomass. Chem Eng J 419:129560. https://doi.org/10.1016/j.cej.2021.129560
12. Matos M, Claro FC, Lima TAM et al (2021) Acetone:water fractionation of pyrolytic lignin improves its antioxidant and antibacterial activity. J Anal Appl Pyrol 156:105175. https://doi.org/10.1016/j.jaap.2021.105175
13. Fortin M, Beromi MM, Lai A et al (2015) Structural analysis of pyrolytic lignins isolated from switchgrass. https://doi.org/10.1021/acs.energyfuels.5b01726. Fast-Pyrolysis Oil
14. Albuquerque BR, Heleno SA, Oliveira MBPP et al (2021) Phenolic compounds: current industrial applications, limitations and future challenges. Food Funct 12:14–29. https://doi.org/10.1039/D0FO02324H
15. Xu Y, Guo L, Zhang H et al (2019) Research status, industrial application demand and prospects of phenolic resin. RSC Adv 9:28924–28935. https://doi.org/10.1039/C9RA06487G
16. Chan YH, Loh SK, Chin BLF et al (2020) Fractionation and extraction of bio-oil for production of greener fuel and value-added chemicals: recent advances and future prospects. Chem Eng J 397:125406. https://doi.org/10.1016/j.cej.2020.125406
17. Li S, Luo Z, Wang W et al (2020) Characterization of pyrolytic lignin and insight into its formation mechanisms using novel techniques and DFT method. Fuel 262:116516. https://doi.org/10.1016/j.fuel.2019.116516
18. Leng F, Wang Y, Chen J et al (2017) Characterization of pyrolytic lignins with different activities obtained from bio-oil. Chin J Chem Eng 25:324–329. https://doi.org/10.1016/j.cjche.2016.06.015
19. Letourneau DR, Volmer DA (2023) Mass spectrometry-based methods for the advanced characterization and structural analysis of lignin: a review. Mass Spectrom Rev 42:144–188. https://doi.org/10.1002/mas.21716
20. Poveda-Giraldo JA, Solarte-Toro JC, Cardona Alzate CA (2021) The potential use of lignin as a platform product in biorefineries: a review. Renew Sustain Energy Rev 138:110688. https://doi.org/10.1016/j.rser.2020.110688
21. Oasmaa A, Kuoppala E, Gust S, Solantausta Y (2003) Fast pyrolysis of forestry residue. 1. Effect of extractives on phase separation of pyrolysis liquids. Energy Fuels 17:1–12. https://doi.org/10.1021/ef020088x
22. Jiang X, Ellis N, Shen DK et al (2012) Thermogravimetry-FTIR analysis of pyrolysis of pyrolytic lignin extracted from bio-oil. Chem Eng Technol 35:827–833. https://doi.org/10.1002/ceat.201000400
23. Oasmaa A, Kuoppala E, Elliott DC (2012) Development of the basis for an analytical protocol for feeds and products of bio-oil hydrotreatment. Energy Fuels 26:2454–2460. https://doi.org/10.1021/ef300252y
24. Santos TM, Silva WR da, Carregosa J, de Wisniewski C (2022) A Comprehensive characterization of cattle manure bio-oil for scale-up assessment comparing non-equivalent reactor designs. Journal of Analytical and Applied Pyrolysis 162:105465. https://doi.org/10.1016/j.jaap.2022.105465
25. Santos JM, Vetere A, Wisniewski A et al (2020) Modified SARA method to unravel the complexity of Resin Fraction(s) in Crude Oil. Energy Fuels 34:16006–16013. https://doi.org/10.1021/acs.energyfuels.0c02833
26. Staš M, Chudoba J, Kubička D et al (2017) Petroleomic characterization of pyrolysis bio-oils: a review. Energy Fuels 31:10283–10299. https://doi.org/10.1021/acs.energyfuels.7b00826

27. Oasmaa A, Kuoppala E, Ardiyanti A et al (2010) Characterization of hydrotreated fast pyrolysis liquids. Energy Fuels 24:5264–5272. https://doi.org/10.1021/ef100573q

28. Yu Y, Chua YW, Wu H (2016) Characterization of pyrolytic sugars in bio-oil produced from biomass fast pyrolysis. Energy Fuels 30:4145–4149. https://doi.org/10.1021/acs.energyfuels.6b00464

29. Bridgwater AV (2012) Review of fast pyrolysis of biomass and product upgrading. Biomass Bioenergy 38:68–94. https://doi.org/10.1016/j.biombioe.2011.01.048

30. Ruiz M, Valette J, Broust F, Bonfils F (2019) Rapid quantification and characterization of the pyrolytic lignin fraction of bio-oils by size exclusion chromatography coupled with multi-angle laser light scattering detector (SEC-MALS). J Anal Appl Pyrol 142:104662. https://doi.org/10.1016/j.jaap.2019.104662

31. Bayerbach R, Meier D (2009) Characterization of the water-insoluble fraction from fast pyrolysis liquids (pyrolytic lignin). Part IV: structure elucidation of oligomeric molecules. J Anal Appl Pyrol 85:98–107. https://doi.org/10.1016/j.jaap.2008.10.021

32. Pienihäkkinen E, Stamatopoulos I, Krassa P et al (2023) Production of pyrolytic lignin for the phenolic resin synthesis via fast pyrolysis. J Anal Appl Pyrol 176:106239. https://doi.org/10.1016/j.jaap.2023.106239

33. Nsimba RY, Mullen CA, West NM, Boateng AA (2013) Structure-property characteristics of pyrolytic lignins derived from fast pyrolysis of a lignin rich biomass extract. ACS Sustainable Chem Eng 1:260–267. https://doi.org/10.1021/sc300119s

34. Boscagli C, Raffelt K, Zevaco TA et al (2015) Mild hydrotreatment of the light fraction of fast-pyrolysis oil produced from straw over nickel-based catalysts. Biomass Bioenergy 83:525–538. https://doi.org/10.1016/j.biombioe.2015.11.003

35. Yu J, Wang D, Sun L (2021) The pyrolysis of lignin: pathway and interaction studies. Fuel 290:120078. https://doi.org/10.1016/j.fuel.2020.120078

36. Lin X, Sui S, Tan S et al (2015) Fast pyrolysis of four lignins from different isolation processes using Py-GC/MS. Energies 8:5107–5121. https://doi.org/10.3390/en8065107

37. Amit TA, Roy R, Raynie DE (2021) Thermal and structural characterization of two commercially available technical lignins for potential depolymerization via hydrothermal liquefaction. Curr Res Green Sustainable Chem 4:100106. https://doi.org/10.1016/j.crgsc.2021.100106

38. Graglia M, Kanna N, Esposito D (2015) Lignin refinery: towards the preparation of renewable aromatic building blocks. https://doi.org/10.1002/cben.201500019. ChemBioEng Reviews n/a-n/a

39. Mullen CA, Boateng AA (2011) Characterization of water insoluble solids isolated from various biomass fast pyrolysis oils. J Anal Appl Pyrol 90:197–203. https://doi.org/10.1016/j.jaap.2010.12.004

40. Wang S, Lin H, Ru B et al (2014) Comparison of the pyrolysis behavior of pyrolytic lignin and milled wood lignin by using TG–FTIR analysis. J Anal Appl Pyrol 108:78–85. https://doi.org/10.1016/j.jaap.2014.05.014

41. Qu W, Xue Y, Gao Y et al (2016) Repolymerization of pyrolytic lignin for producing carbon fiber with improved properties. Biomass Bioenergy 95:19–26. https://doi.org/10.1016/j.biombioe.2016.09.013

42. Sajid M, Justyna P (2018) Green nature of the process of derivatization in analytical sample preparation. Trends Anal Chem 102:16–31. https://doi.org/10.1016/j.trac.2018.01.005

43. Zhang X, Ma H, Wu S, Wei W (2019) Sequential fractionation of lignin-derived pyrolysis oil via extraction with a combination of water and organic solvents. BioResources 14:2144–2159. https://doi.org/10.15376/biores.14.1.2144-2159

44. Tarasov D, Leitch M, Fatehi P (2018) Lignin–carbohydrate complexes: properties, applications, analyses, and methods of extraction: a review. Biotechnol Biofuels 11:269. https://doi.org/10.1186/s13068-018-1262-1

45. Scholze B, Hanser C, Meier D (2001) Characterization of the water-insoluble fraction from fast pyrolysis liquids (pyrolytic lignin). J Anal Appl Pyrol 58–59:387–400. https://doi.org/10.1016/S0165-2370(00)00173-X

46. Laskar DD, Zeng J, Yan L et al (2013) Characterization of lignin derived from water-only flowthrough pretreatment of Miscanthus. Ind Crops Prod 50:391–399. https://doi.org/10.1016/j.indcrop.2013.08.002

47. Scholze B, Meier D (2001) Characterization of the water-insoluble fraction from pyrolysis oil (pyrolytic lignin). Part I. PY–GC/MS, FTIR, and functional groups. J Anal Appl Pyrol 60:41–54. https://doi.org/10.1016/S0165-2370(00)00110-8

48. Lima CF, Barbosa LCA, Silva MNN et al (2015) In situ determination of the syringyl/guaiacyl ratio of residual lignin in pre-bleached eucalypt kraft pulps by analytical pyrolysis. J Anal Appl Pyrol 112:164–172. https://doi.org/10.1016/j.jaap.2015.02.002

49. Ibarra D, del Río JC, Gutiérrez A et al (2005) Chemical characterization of residual lignins from eucalypt paper pulps. J Anal Appl Pyrol 74:116–122. https://doi.org/10.1016/j.jaap.2004.12.009

50. Chen W, McClelland DJ, Azarpira A et al (2016) Low temperature hydrogenation of pyrolytic lignin over Ru/TiO 2: 2D HSQC and 13 C NMR study of reactants and products. Green Chem 18:271–281. https://doi.org/10.1039/C5GC02286J

51. Yuan T-Q, Sun S-N, Xu F, Sun R-C (2011) Characterization of lignin structures and lignin–carbohydrate complex (LCC) linkages by quantitative 13 C and 2D HSQC NMR spectroscopy. J Agric Food Chem 59:10604–10614. https://doi.org/10.1021/jf2031549

52. Suota MJ, da Silva TA, Zawadzki SF et al (2021) Chemical and structural characterization of hardwood and softwood Ligno-Force™ lignins. Ind Crops Prod 173:114138. https://doi.org/10.1016/j.indcrop.2021.114138

53. Rosado MJ, Rencoret J, Marques G et al (2021) Structural characteristics of the guaiacyl-rich lignins from rice (Oryza sativa L.) husks and straw. Front Plant Sci 12. https://doi.org/10.3389/fpls.2021.640475

54. Hossain MA, Phung TK, Rahaman MS et al (2019) Catalytic cleavage of the β-O-4 aryl ether bonds of lignin model compounds by Ru/C catalyst. Appl Catal A 582:117100. https://doi.org/10.1016/j.apcata.2019.05.034

55. Zhu X, Sipilä J, Potthast A et al (2023) Exploring alkyl-o-alkyl ether structures in softwood milled wood lignins. J Agric Food Chem 71:580–591. https://doi.org/10.1021/acs.jafc.2c06375

56. Hertzog J, Carré V, Aubriet F (2019) Contribution of Fourier transform mass spectrometry to bio-oil study. In: Fundamentals and applications of Fourier Transform Mass Spectrometry. Elsevier, pp 679–733

57. Terrell E, Garcia-Perez M (2020) Vacuum pyrolysis of hybrid poplar milled wood lignin with fourier transform-ion cyclotron resonance mass spectrometry analysis of feedstock and products for

the elucidation of reaction mechanisms. Energy Fuels 34:14249–14263. https://doi.org/10.1021/acs.energyfuels.0c02928

58. Asare SO, Huang F, Lynn BC (2019) Characterization and sequencing of lithium cationized β-O-4 lignin oligomers using higher-energy collisional dissociation mass spectrometry. Anal Chim Acta 1047:104–114. https://doi.org/10.1016/j.aca.2018.09.068

59. Prothmann J, Spégel P, Sandahl M, Turner C (2018) Identification of lignin oligomers in Kraft lignin using ultra-high-performance liquid chromatography/high-resolution multiple-stage tandem mass spectrometry (UHPLC/HRMSn). Anal Bioanal Chem 410:7803–7814. https://doi.org/10.1007/s00216-018-1400-4